AIAA JOURNAL
Vol. 36, No. 8, August 1998

Dynamic Modeling of a Smart Materials Robot

S. S. Ge,* T. H. Lee,† and J. Q. Gong‡
National University of Singapore, 119260 Singapore

Three dynamic models of a smart materials robot are presented. First, Hamilton's approach is adopted to derive an accurate model expressed in partial differential equations, which is too complicated to be applicable in engineering practice. Based on the partial differential equations model, the assumed modes method and the finite element method are employed to derive two finite dimensional models in the forms of ordinary differential equations, which are readily usable for controller design. All of the models show that the model of a smart materials robot cannot be simply taken to be the same as that of a pure flexible robot, and the parameters of the smart materials robot should be properly chosen to avoid the divergent open-loop responses. For completeness, both mechanical dynamics and electrical dynamics are explicitly included in all of these models, although it is shown analytically and numerically that the latter dynamics can be omitted in engineering applications. Comparative studies between the assumed modes method model and the finite element method model are carried out by numerical simulations in both time and frequency domains to verify the correctness of the models and to analyze the performance of the system.

Nomenclature

a = thicknesses of the beam
$\boldsymbol{B}$ = magnetic flux density vector, $\in R^3$
b = width of the beam and that of the smart materials
$\boldsymbol{C}_A$ = centripetal/Coriolis matrix in the assumed modes method (AMM) model
c_L = stiffness per unit length of the smart materials robot, $\frac{1}{3}b\{(c_{11}^M a^3/4) + c_{11}^S[(a/2 + c_1)^3 + (a/2 + c_2)^3 - a^3/4]\}$
c_1 = thicknesses of upper surface of smart materials plate
c_2 = thicknesses of the lower surface of smart materials plate
$\boldsymbol{c}^M$ = symmetric matrix of elastic stiffness coefficients of the pure beam, $\in R^{6\times 6}$
$\boldsymbol{c}^S$ = symmetric matrix of elastic stiffness coefficients of the smart materials, $\in R^{6\times 6}$
c_{11}^M = stiffness of the pure beam
c_{11}^S = stiffness of the piezoelectric materials
$\boldsymbol{D} \in R^3$ = electrical displacement vector
$D(x, t)$ = electrical displacement at point P
d_{ia}, d_{ib} = electrical displacements at nodes a and b of element i
E_k = system kinetic energy
E_p = system potential energy
$\boldsymbol{E} \in R^3$ = electrical field intensity vector
$\boldsymbol{F}_A \in R^{N+1}$ = external force vector in the AMM model
$\boldsymbol{F}^M \in R^6$ = simplified stress vector of the pure beam
$\boldsymbol{F}^S \in R^6$ = simplified stress vector of the smart materials
$\boldsymbol{H}$ = magnetic field intensity vector, $\in R^3$
$H(x, t)$ = magnetic field intensity at point P
$\boldsymbol{h}$ = coupling coefficients matrix, $\in R^{6\times 3}$
h_L = coupling parameter per unit length of the smart materials robot, $\frac{1}{2}h_{12}b(c_1 - c_2)(c_1 + c_2 + a)$
I_h = inertia of the hub
i = number of the order of element
$\boldsymbol{K}_A$ = stiffness matrix in the AMM model
$\boldsymbol{M}_A$ = inertia matrix in the AMM model
m_3 = tip payload
N = number of the modes in the AMM modeling or number of finite elements in the finite element method (FEM) modeling
$\boldsymbol{o}_i$ = position vector of origin of the ith frame expressed in the fixed-base frame
$\boldsymbol{p}_i$ = position vector from $\boldsymbol{o}_i$ to point P expressed in the fixed-base frame
$\boldsymbol{r}$ = position vector of point P expressed in the fixed-base frame (for the AMM modeling)
$\boldsymbol{r}_i$ = position vector of the point P expressed in the fixed-base frame (for the FEM modeling)
$\boldsymbol{S} \in R^6$ = simplified strain vector
$\boldsymbol{T} \in R^{N+1}$ = nonconservative generalized force vector applied to the system
v_{ia}, v_{ib} = linear displacements at nodes a and b of element i
W = virtual work done by the nonconservative forces
$w(x, t)$ = deflection at point P
w_i = deflection at point P of element i
(X, O, Y) = local reference frame with axis OX being tangent to the beam at the base
(X_0, O_0, Y_0) = fixed-base frame
(x_i, o_i, y_i) = local reference frame of element i
$\boldsymbol{\beta}$ = symmetric matrix of impermittivity coefficients, $\in R^{3\times 3}$
β_L = impermittivity per unit length of the smart materials robot, $b(c_1 + c_2)\beta_{22}$
$\theta(t)$ = joint angle at the hub
$\boldsymbol{\mu}$ = permeability coefficients matrix, $\in R^{3\times 3}$
μ_L = permeability per unit length of the smart materials robot, $b(c_1 + c_2)\mu_{33}$
ρ_L = mass per unit length of the smart materials robot, $(c_1 + c_2)b\rho_2 + ab\rho_1$
ρ_1 = mass per unit volume of pure beam
ρ_2 = mass per unit volume of smart materials
ϕ_{ia}, ϕ_{ib} = rotational displacements at nodes a and b of element i
$\psi_i(x)$ = the ith modes shape function or the eigenfunction

Received June 13, 1997; revision received April 3, 1998; accepted for publication April 3, 1998.

*Lecturer, Department of Electrical Engineering, 10 Kent Ridge Crescent.
†Associate Professor, Department of Electrical Engineering, 10 Kent Ridge Crescent.
‡Research Student, Department of Electrical Engineering, 10 Kent Ridge Crescent.

Introduction

BOTH the rigid-body and elastic deformations should be precisely controlled in the mission of flexible space structures. According to current thinking, a small number of high-authority actuators are attached to the host structure to achieve this task.[1–4] It requires that the modes of the system be known to a high degree of accuracy, which is actually very tough because accurate dynamics for a large space structure are hard to obtain.

An alternative approach is the use of a smart structure, i.e., a structure with networks of highly distributed actuators, sensors, and

processors. Such a system allows the distributed control strategies to be easily implementable, though it cannot be implemented by a small number of sensors and actuators. Piezoelectric materials are readily available to serve as actuators and sensors in this distributed control approach because of their unique properties to achieve the transformation between the mechanical and electrical energies. Much theoretical and experimental work to investigate the properties of a beam attached by piezoelectric materials[5–9] has been reported in the literature. Pioneering research work has been carried out in Ref. 5 on the modeling of smart structures. The effects of dynamic couplings between the host structure and piezoelectric materials were examined. Dynamic models have been developed and experimentally verified for three important cases: direct-voltage-driven electrodes, direct-current-driven electrodes, and indirect drive cases. From the basic piezoelectric stress-strain relationship, static and dynamic analytic models were derived for segmented piezoelectric actuators that were bonded to an elastic substructure or embedded in a laminate composite.[6] Based on the conventional Euler–Bernoulli beam theory, the model of a beam with its upper surface covered by piezoelectric materials was derived from a dynamic force balance point of view in Ref. 7. The model in Ref. 7 and its series solution were developed from a virtual work approach in Ref. 8. The interactions between the host structure and the smart materials were discussed in Ref. 9, which showed that the mechanical properties of smart materials should be considered in the modeling of a smart materials beam.

In this paper, a flexible link robot covered by two piezoelectric plates on both surfaces is discussed. Three models for this smart materials robot are obtained systematically. To obtain a full model with both electrical dynamics and mechanical dynamics, both electrical and mechanical properties of the smart materials (rather than the piezoelectric stress-strain relationship only) and mechanical properties of the flexible robot are taken into consideration. First, Hamilton's approach is used to derive a theoretical model in the form of partial differential equations (PDEs), which is too complicated to be applicable in engineering practice. Then an assumed modes method (AMM) and a finite element method (FEM) are used in association with the Lagrange approach to obtain two approximated finite dimensional models in forms of ordinary differential equations (ODEs). These two approximated models can be written in the conventional state-space forms, for which advanced controller design can be investigated. Based on these models, the system performance of a smart materials robot is discussed.

The rest of the paper is organized as follows. First, fundamental concepts and equations of piezoelectric materials robots are briefly described. Second, Hamilton's approach is discussed in detail. Third, models based on AMM and FEM, respectively, are developed. Finally, the comparative simulation studies are carried out, followed by a conclusion.

Fundamentals of Piezoelectric Materials Robots

Piezoelectric materials are a special kind of material that can realize the energy transformation between mechanical energy and electrical energy. To introduce the dynamics of the electrical quantities, we will consider all of the mechanical energy, electrical energy, and magnetic energy.

In this paper, superscript M is used for the mechanical quantities, E for the electrical quantities, C for the coupled quantities, and S for the quantities related to the smart materials.

We have the following fundamental relationships.

1) Piezoelectric effects[10]:

$$\boldsymbol{F}^S = \boldsymbol{c}^S \boldsymbol{S} - \boldsymbol{h}\boldsymbol{D} \tag{1}$$

$$\boldsymbol{E} = -\boldsymbol{h}^T \boldsymbol{S} + \boldsymbol{\beta}\boldsymbol{D} \tag{2}$$

2) Magnetic properties, neglecting the piezomagnetic effects:

$$\boldsymbol{B} = \boldsymbol{\mu}\boldsymbol{H} \tag{3}$$

3) Mechanical properties of the pure beam:

$$\boldsymbol{F}^M = \boldsymbol{c}^M \boldsymbol{S} \tag{4}$$

Modeling with Hamilton's Approach

System Structure and Basic Assumption

The flexible robot under study is enveloped by two plates of piezoelectric materials, which can act as actuators or sensors for better controller performance. One end of the beam is rigidly attached to the rotor of a motor in the horizontal plane. Thus, the effect of gravity is neglected.

It is assumed that only the motor torque is applied to the hub and the tip payload is considered as a point mass. The schematics of the system are shown in Fig. 1, and the geometry of the system is shown in Fig. 2.

From Fig. 2, it is easily found that, except for the joint angle, which is a function of time t only, all functions depend on both x and t, and their definition domains are $[0, L] \times [0, \infty]$ unless otherwise stated.

In this paper, we make the standard assumption of small deflection. As shown in Fig. 2, electrical displacement $D(x, t)$ is perpendicular to the beam in the plane of XOY. Thus its z component $D_z = 0$. Moreover, due to the small deflection, we have $D_x \ll D_y$; therefore, we assume that $D_x = 0$. The magnetic field intensity H is perpendicular to the plane XOY; consequently, $H_x = H_y = 0$. We will be concerned about only D_y and H_z in the following discussion.

Kinetic Energy

The kinetic energy includes two parts: the mechanical kinetic energy and the electrical kinetic energy. The latter is actually the magnetic energy. It is called electrical kinetic energy here because it is related to the time derivative of the electrical displacement and is independent of the electrical displacement,[11] which will be shown later on. In the following derivation, we assume that the length of the beam is constant.

First, the mechanical kinetic energy is derived. The position vector $\boldsymbol{r}$ of a point P on the beam can be expressed in the fixed-base frame as

$$\boldsymbol{r} = \begin{bmatrix} \cos\theta & -\sin\theta \\ \sin\theta & \cos\theta \end{bmatrix} \begin{bmatrix} x \\ w(x, t) \end{bmatrix} \tag{5}$$

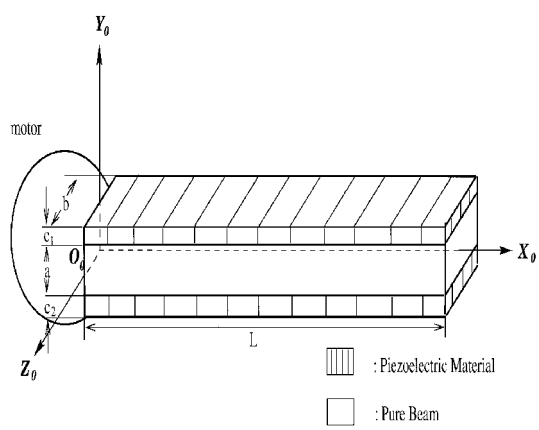

Fig. 1 Structure of the flexible link robot enveloped with piezoelectric materials.

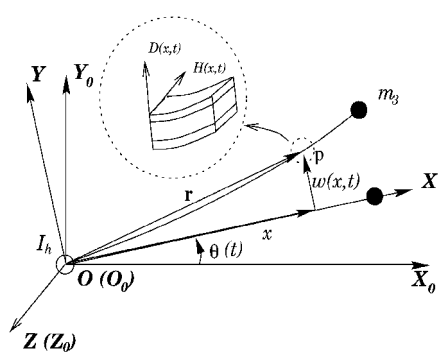

Fig. 2 Coordinate systems of the smart materials robot.

and we have

$$\dot{\boldsymbol{r}} = \frac{\mathrm{d}\boldsymbol{r}}{\mathrm{d}t} = \begin{bmatrix} \dfrac{\mathrm{d}}{\mathrm{d}t}(x\cos\theta - w(x,t)\sin\theta) \\ \dfrac{\mathrm{d}}{\mathrm{d}t}(x\sin\theta + w(x,t)\cos\theta \end{bmatrix}$$

$$= \begin{bmatrix} \cos\theta & -\sin\theta \\ \sin\theta & \cos\theta \end{bmatrix} \begin{bmatrix} \dot{x} - w(x,t)\dot{\theta} \\ \dot{\theta}x + \dot{w}(x,t) \end{bmatrix}$$

$$= \begin{bmatrix} \cos\theta & -\sin\theta \\ \sin\theta & \cos\theta \end{bmatrix} \begin{bmatrix} -w(x,t)\dot{\theta} \\ \dot{\theta}x + \dot{w}(x,t) \end{bmatrix} \tag{6}$$

where $\dot{x} = 0$ because the length of the beam is assumed to be a constant.

The mechanical kinetic energy is then given by

$$E_k^M = \frac{1}{2} I_h \dot{\theta}^2 + \frac{(c_1 + c_2) b \rho_2 + ab\rho_1}{2} \int_0^L \dot{\boldsymbol{r}}^T(x,t)\dot{\boldsymbol{r}}(x,t)\,\mathrm{d}x$$

$$+ \frac{m_3}{2}\dot{\boldsymbol{r}}^T(L,t)\dot{\boldsymbol{r}}(L,t) = \frac{1}{2} I_h \dot{\theta}^2 + \frac{\rho_L}{2}$$

$$\times \left(\frac{L^3}{3}\dot{\theta}^2 + \int_0^L \{[-w(x,t)\dot{\theta}]^2 + 2x\dot{\theta}\dot{w}(x,t) + \dot{w}^2(x,t)\}\,\mathrm{d}x \right)$$

$$+ \frac{m_3}{2}\{[w(L,t)\dot{\theta}]^2 + [L\dot{\theta} + \dot{w}(L,t)]^2\} \tag{7}$$

The first term on the right-hand side of Eq. (7) is the kinetic energy of the hub, the second term is that of the smart materials beam, and the third term is that of the payload.

The electrical kinetic energy, i.e., magnetic energy, is derived as follows.

According to the Maxwell equation,[12]

$$\nabla \times \boldsymbol{H} = \frac{\partial \boldsymbol{D}}{\partial t} \tag{8}$$

and recalling that $D_x = D_z = 0$, $H_x = H_y = 0$, as stated in the preceding subsection, the equation of H_z can be written as

$$H_z(x,t) = -\int_0^x \dot{D}_y(\xi,t)\,\mathrm{d}\xi \tag{9}$$

We can see that $H_z(x,t)$ is a function of the time derivative of $D_y(x,t)$. Thus, the magnetic energy is looked on as the electrical kinetic energy, which is in the form

$$E_k^E = \frac{b(c_1 + c_2)\mu_{33}}{2} \int_0^L \left[\int_0^x \dot{D}_y(\xi,t)\,\mathrm{d}\xi \right]^2 \mathrm{d}x$$

$$= \frac{\mu_L}{2} \int_0^L \left[\int_0^x \dot{D}_y(\xi,t)\,\mathrm{d}\xi \right]^2 \mathrm{d}x \tag{10}$$

The total kinetic energy of the system is the sum of mechanical kinetic energy and electrical kinetic energy, i.e.,

$$E_k = E_k^M + E_k^E \tag{11}$$

Potential Energy

Recalling that the robot is in the horizontal plane, we do not include gravitational energy.

Before calculating the mechanical potential energy, a strain calculation is in order[13]:

$$S_1 = -y\frac{\partial^2 w(x,t)}{\partial x^2}, \qquad S_2 = S_3 = S_4 = S_5 = S_6 = 0$$

The total potential energy is given by

$$E_p = \frac{1}{2} b \int_0^L \int_{-\frac{a}{2} - c_2}^{-\frac{a}{2}} [\boldsymbol{S}^T \boldsymbol{F}^S + \boldsymbol{E}^T \boldsymbol{D}]\,\mathrm{d}y\,\mathrm{d}x$$

$$+ \frac{1}{2} b \int_0^L \int_{-\frac{a}{2}}^{\frac{a}{2}} \boldsymbol{S}^T \boldsymbol{F}^M\,\mathrm{d}y\,\mathrm{d}x$$

$$+ \frac{1}{2} b \int_0^L \int_{\frac{a}{2}}^{\frac{a}{2} + c_1} [\boldsymbol{S}^T \boldsymbol{F}^S + \boldsymbol{E}^T \boldsymbol{D}]\,\mathrm{d}y\,\mathrm{d}x$$

$$= \frac{b}{2}\left(\frac{1}{3}\left\{ \frac{c_{11}^M a^3}{4} + c_{11}^S \left[\left(\frac{a}{2} + c_1\right)^3 + \left(\frac{a}{2} + c_2\right)^3 - \frac{a^3}{4} \right] \right\} \right.$$

$$\times \int_0^L \left[\frac{\partial^2 w(x,t)}{\partial x^2} \right]^2 \mathrm{d}x + (c_1 + c_2)\beta_{22} \int_0^L D_y^2(x,t)\,\mathrm{d}x$$

$$\left. + \frac{1}{2} h_{12}(c_1 - c_2)(c_1 + c_2 + a) \int_0^L D_y(x,t) \frac{\partial^2 w(x,t)}{\partial x^2}\,\mathrm{d}x \right)$$

$$= \frac{c_L}{2} \int_0^L \left[\frac{\partial^2 w(x,t)}{\partial x^2} \right]^2 \mathrm{d}x + \frac{\beta_L}{2} \int_0^L D_y^2(x,t)\,\mathrm{d}x$$

$$+ h_L \int_0^L D_y(x,t) \frac{\partial^2 w(x,t)}{\partial x^2}\,\mathrm{d}x \tag{12}$$

From Eq. (12), it can be found that the potential energy includes three parts: the mechanical potential energy, the electrical potential energy, and the coupled potential energy.

Virtual Work

The virtual work includes two parts: the mechanical virtual work, which is from the motor torque, and the electrical virtual work, which is done by the voltages exerted on the smart materials actuators. We will derive them successively.

The mechanical virtual work is in the form

$$\delta W^M = \tau \delta \frac{\partial w(0,t)}{\partial x} + \tau \delta\theta \tag{13}$$

Assuming that the applied voltage is a function of both x and t, the electrical virtual work is obtained:

$$\delta W^E = \int_0^L bV(x,t)\delta D_y(x,t)\,\mathrm{d}x \tag{14}$$

The total virtual work is then given by

$$\delta W = \delta W^M + \delta W^E \tag{15}$$

Hamilton's Approach

The celebrated Hamilton's principle is described as[14]

$$\delta \int_{t_0}^{t_1} (E_k - E_p + W)\,\mathrm{d}t = 0 \tag{16}$$

where $\delta(\,)$ denotes the variational operator.

In deriving the model by Hamilton's approach, the following conditions are used:

$$\begin{gathered} \delta x = 0 \\ \frac{\mathrm{d}^n x}{\mathrm{d}t^n} \equiv 0, \qquad n = 1, 2, 3, \ldots \\ \delta\theta(t_0) = \delta\theta(t_1) = 0 \\ \delta w(x,t_0) = \delta w(x,t_1) = 0 \\ \delta D_y(x,t_0) = \delta D_y(x,t_1) = 0 \\ \delta w(0,t) = 0, \qquad \frac{\partial}{\partial x}\delta w(0,t) = 0 \end{gathered} \tag{17}$$

where the first two conditions are due to the constant length of the beam, the following three conditions are standard assumptions that

variations vanish at the two endpoints corresponding to $t = t_0$ and t_1, the last two conditions hold because the beam is fixed at $x = 0$, and the local reference frame is selected such that axis OX is tangent to the beam at the base.

Substituting Eqs. (11–15) into the left-hand side of Eq. (16), invoking the conditions in Eq. (17), and integrating by parts, we arrive at

$$\begin{aligned}
&\int_{t_0}^{t_1} \delta(E_k - E_p + W)\,\mathrm{d}t \\
&= \int_{t_0}^{t_1} P_1 \delta\theta\,\mathrm{d}t + \int_{t_0}^{t_1}\int_0^L P_2 \delta w(x,t)\,\mathrm{d}x\,\mathrm{d}t \\
&+ \int_{t_0}^{t_1}\int_0^L P_3 \delta D_y(x,t)\,\mathrm{d}x\,\mathrm{d}t + \int_{t_0}^{t_1} P_4 \delta w(L,t)\,\mathrm{d}t \\
&+ \int_{t_0}^{t_1} P_5 \frac{\partial}{\partial x}\delta w(L,t)\,\mathrm{d}t + \int_{t_0}^{t_1} P_6 \int_0^L \delta D_y(\xi,t)\,\mathrm{d}\xi\,\mathrm{d}t \qquad (18)
\end{aligned}$$

where

$$\begin{aligned}
P_1 &= \left(-I_h - \frac{L^3\rho_L}{3}\right)\ddot{\theta} - \rho_L \int_0^L [2w(x,t)\dot{w}(x,t)\dot{\theta} \\
&\quad + w^2(x,t)\ddot{\theta} + x\ddot{w}(x,t)]\,\mathrm{d}x - m_3[2w(L,t)\dot{w}(L,t)\dot{\theta} \\
&\quad + w^2(L,t)\ddot{\theta} + L^2\ddot{\theta} + L\ddot{w}(L,t)] + \tau \\
P_2 &= \rho_L[w(x,t)\dot{\theta}^2 - x\ddot{\theta} - \ddot{w}(x,t)] \\
&\quad - c_L\frac{\partial^4 w(x,t)}{\partial x^4} - h_L\frac{\partial^2 D_y(x,t)}{\partial x^2} \\
P_3 &= \mu_L \int_0^x \int_0^\xi \ddot{D}_y(\zeta,t)\,\mathrm{d}\zeta\,\mathrm{d}\xi - \beta_L D_y(x,t) \qquad (19) \\
&\quad - h_L\frac{\partial^2 w(x,t)}{\partial x^2} + bV(x,t) \\
P_4 &= m_3[w(L,t)\dot{\theta}^2 - L\ddot{\theta} - \ddot{w}(L,t)] \\
&\quad + c_L\frac{\partial^3 w(L,t)}{\partial x^3} + h_L\frac{\partial D_y(L,t)}{\partial x} \\
P_5 &= -c_L\frac{\partial^2 w(L,t)}{\partial x^2} - h_L D_y(L,t) \\
P_6 &= -\mu_L \int_0^L \int_0^x \ddot{D}_y(\xi,t)\,\mathrm{d}\xi\,\mathrm{d}x
\end{aligned}$$

which, to satisfy Eq. (16), yields the PDEs

$$\begin{aligned}
&\left(I_h + \frac{L^3\rho_L}{3}\right)\ddot{\theta} + \rho_L \int_0^L [2w(x,t)\dot{w}(x,t)\dot{\theta} + w^2(x,t)\ddot{\theta} \\
&\quad + x\ddot{w}(x,t)]\,\mathrm{d}x + m_3[2w(L,t)\dot{w}(L,t)\dot{\theta} + w^2(L,t)\ddot{\theta} \\
&\quad + L^2\ddot{\theta} + L\ddot{w}(L,t)] = \tau \qquad (20)
\end{aligned}$$

$$\rho_L[w(x,t)\dot{\theta}^2 - x\ddot{\theta} - \ddot{w}(x,t)] = c_L\frac{\partial^4 w(x,t)}{\partial x^4} + h_L\frac{\partial^2 D_y(x,t)}{\partial x^2} \qquad (21)$$

$$\mu_L \int_0^x \int_0^\xi \ddot{D}_y(\zeta,t)\,\mathrm{d}\zeta\,\mathrm{d}\xi = \beta_L D_y(x,t) + h_L\frac{\partial^2 w(x,t)}{\partial x^2} - bV(x,t) \qquad (22)$$

and boundary conditions (BCs)

$$w(0,t) = 0 \qquad (23)$$

$$\frac{\partial w(0,t)}{\partial x} = 0 \qquad (24)$$

$$\begin{aligned}
&m_3[w(L,t)\dot{\theta}^2 - L\ddot{\theta} - \ddot{w}(L,t)] + c_L\frac{\partial^3 w(L,t)}{\partial x^3} \\
&\quad + h_L\frac{\partial D_y(L,t)}{\partial x} = 0 \qquad (25)
\end{aligned}$$

$$c_L\frac{\partial^2 w(L,t)}{\partial x^2} + h_L D_y(L,t) = 0 \qquad (26)$$

$$\mu_L \int_0^L \int_0^x \ddot{D}_y(\xi,t)\,\mathrm{d}\xi\,\mathrm{d}x = 0 \qquad (27)$$

Equation (20) illustrates the moment balance at the base of the robot, Eq. (21) represents the dynamics of vibration of the smart materials robot, and Eq. (22) is the dynamics of the electrical displacement. Conditions (23) and (24) hold because the beam is fixed at $x = 0$, and the local reference frame XOY is selected such that axis OX is tangent to the beam at the base. Equation (21) is related to Eq. (22) through term $h_L[\partial^2 D_y(x,t)/\partial x^2]$, Eq. (22) is related to Eq. (21) through term $h_L[\partial^2 w(x,t)/\partial x^2]$, and BCs (25) and (26) are also related to each other. However, all of these relativenesses, dynamics of the electrical displacement (22), and BC (27) do not exist in the model of a pure flexible robot. As a matter of fact, only when $D_y \equiv 0$, $h_L \equiv 0$, and $V \equiv 0$ does the dynamic model of a smart materials robot degrade to that of a pure flexible robot.

After some simplifications, e.g., $D_y(x,t) = 0$, $V(x,t) = V(t)$, $\dot{\theta}^2 = 0$, and $\ddot{\theta} = 0$, the dynamics of the deflection will become the same form as that in Ref. 7 under the assumption that the moment of inertia of the tip payload is zero. It is clear that the model described by Eqs. (20–27) is infinite dimensional and is too complicated to be directly used for controller design. Therefore, the following two sections are dedicated to the derivation of two approximated finite dimensional models by AMM and FEM, respectively.

AMM Modeling

Due to the assumption of small deflection, arc approximation[4]

$$\boldsymbol{r} = x\theta + w(x,t) \qquad (28)$$

is used to simplify the model stated in the preceding section. Because μ_L is so small (usually in the range of 10^{-12}–10^{-9}), that item

$$\mu_L \int_0^x \int_0^\xi \ddot{D}_y(\zeta,t)\,\mathrm{d}\zeta\,\mathrm{d}\xi$$

in Eq. (22) can be taken as zero, and condition (27) can be removed. After these simplifications, we arrive at a simplified model:

$$\left(I_h + \frac{L^3\rho_L}{3}\right)\ddot{\theta} + \rho_L \int_0^L [x\ddot{w}(x,t)]\,\mathrm{d}x + m_3[L^2\ddot{\theta} + L\ddot{w}(L,t)] = \tau \qquad (29)$$

$$-\rho_L[x\ddot{\theta} + \ddot{w}(x,t)] = \left(c_L - \frac{h_L^2}{\beta_L}\right)\frac{\partial^4 w(x,t)}{\partial x^4} + \frac{h_L b}{\beta_L}\frac{\partial^2 V(x,t)}{\partial x^2} \qquad (30)$$

$$D_y(x,t) = -\frac{h_L}{\beta_L}\frac{\partial^2 w(x,t)}{\partial x^2} + \frac{b}{\beta_L}V(x,t) \qquad (31)$$

with BCs

$$w(0,t) = 0, \qquad \frac{\partial w(0,t)}{\partial x} = 0$$

$$\left(c_L - \frac{h_L^2}{\beta_L}\right)\frac{\partial^3 w(L,t)}{\partial x^3} + \frac{h_L b}{\beta_L}\frac{\partial V(L,t)}{\partial x} = m_3[L\ddot{\theta} + \ddot{w}(L,t)] \qquad (32)$$

$$\left(c_L - \frac{h_L^2}{\beta_L}\right)\frac{\partial^2 w(L,t)}{\partial x^2} = \frac{h_L b}{\beta_L}V(L,t)$$

For the convenience of derivation, it will be temporarily assumed that $V(x,t) = 0$, and this assumption will be removed later in the discussion. A constrained modes method is applied, which means

$\ddot{\theta} = 0$. Under these assumptions, a further simplified boundary problem is obtained.

1) Equations:

$$-\rho_L \ddot{w}(x,t) = \left(c_L - \frac{h_L^2}{\beta_L}\right)\frac{\partial^4 w(x,t)}{\partial x^4} \tag{33}$$

$$D_y(x,t) = -\frac{h_L}{\beta_L}\frac{\partial^2 w(x,t)}{\partial x^2} \tag{34}$$

2) BCs:

$$w(0,t) = 0, \qquad \frac{\partial w(0,t)}{\partial x} = 0, \qquad \frac{\partial^2 w(L,t)}{\partial x^2} = 0 \tag{35}$$

$$m_3 \ddot{w}(L,t) = \left(c_L - \frac{h_L^2}{\beta_L}\right)\frac{\partial^3 w(L,t)}{\partial x^3}$$

To solve Eq. (33) under conditions (35), we invoke the variable separation method; thus the solution of Eq. (33) is assumed to be of the form[15]

$$w(x,t) = \Psi(x)Q(t) \tag{36}$$

Substituting this equation into Eq. (33), we have

$$\frac{\Psi''''(x)}{\Psi(x)} \cdot \frac{c_L\beta_L - h_L^2}{\rho_L\beta_L} = -\frac{\ddot{Q}(t)}{Q(t)} \tag{37}$$

where primes denote the derivatives of x and dots denote the derivatives of t. It is clear that the left-hand side of Eq. (37) is a function of x only, whereas the right-hand side depends only on t. Therefore, both sides of Eq. (37) should be equal to a constant. If k is used to denote the constant, PDE (37) can be reduced into two ODEs, namely,

$$\ddot{Q}(t) = -kQ(t) \tag{38}$$

$$\Psi''''(x) = \frac{\rho_L\beta_L}{c_L\beta_L - h_L^2}k\Psi(x) \tag{39}$$

and the BCs (35) become

$$\Psi(0) = 0, \qquad \Psi'(0) = 0, \qquad \Psi''(L) = 0$$

$$\Psi'''(L) = \frac{m_3\beta_L}{h_L^2 - c_L\beta_L}k\Psi(L) \tag{40}$$

It is easy to show that $k = 0$ and $k[\rho_L\beta_L/(c_L\beta_L - h_L^2)] < 0$ will lead to trivial solutions. Thus, we will consider the condition

$$k\frac{\rho_L\beta_L}{c_L\beta_L - h_L^2} > 0 \tag{41}$$

Equation (39) can be rewritten as

$$\Psi''''(x) = (\nu/L)^4\Psi(x) \tag{42}$$

with

$$\left(\frac{\nu}{L}\right)^4 = k\frac{\rho_L\beta_L}{c_L\beta_L - h_L^2} \tag{43}$$

The general solution to Eq. (42) is of the form

$$\Psi(x) = C_1\cos(\nu x/L) + C_2\cosh(\nu x/L) + C_3\sin(\nu x/L) + C_4\sinh(\nu x/L) \tag{44}$$

From BCs (40), a set of equations is obtained:

$$C_1 + C_2 = 0, \qquad C_3 + C_4 = 0$$

$$-C_1\cos\nu + C_2\cosh\nu - C_3\sin\nu - C_4\sinh\nu = 0$$

$$C_1[\sin\nu + (m_3\nu/\rho_L L)\cos\nu] + C_2[\sinh\nu + (m_3\nu/\rho_L L)\cosh\nu]\cosh\nu + C_3[(m_3\nu/\rho_L L)\sin\nu - \cos\nu] + C_4[\cosh\nu + (m_3\nu/\rho_L L)\sinh\nu] = 0 \tag{45}$$

To obtain nontrivial solutions, the determinant of the coefficient matrix of Eqs. (45) must be zero, i.e.,

$$1 + \cosh\nu\cos\nu + (m_3\nu/\rho_L L)(\sinh\nu\cos\nu - \cosh\nu\sin\nu) = 0 \tag{46}$$

which may be satisfied by an infinite number of ν. Note that only positive ν are used. Therefore it is possible to avoid trivial solutions only when condition (41) is satisfied. As for condition (41), because ρ_L and β_L are positive constants, three cases exist.

1) Case 1:

$$k > 0, \qquad c_L\beta_L - h_L^2 > 0 \tag{47}$$

2) Case 2:

$$k < 0, \qquad c_L\beta_L - h_L^2 < 0 \tag{48}$$

3) Case 3:

$$k > 0, \qquad c_L\beta_L - h_L^2 = 0 \tag{49}$$

In the first case, $k > 0$ is required, and it can be found that the solution to Eq. (38) is harmonic. In the second case, however, the solution to Eq. (38) will be divergent because $k < 0$. From the preceding analysis, one can see that the parameters of the smart materials robot are directly related to the performance of the system. This result can also be derived from the FEM modeling later. In the third case, because $c_L\beta_L - h_L^2 = 0$, Eq. (33) and conditions (35) become the following.

Equation:

$$-\rho_L\ddot{w}(x,t) = 0$$

BCs:

$$w(0,t) = 0, \qquad \frac{\partial w(0,t)}{\partial x} = 0$$

$$\frac{\partial^2 w(L,t)}{\partial x^2} = 0, \qquad m_3\ddot{w}(L,t) = 0$$

which clearly leads to a trivial solution. Therefore, to avoid a divergent solution and a trivial solution, it is assumed that $c_L\beta_L - h_L^2 > 0$ and $k > 0$ from now on.

Considering the first three equations in Eqs. (45), the general solution (44) can be rewritten as

$$\Psi(x) = C_2\{\cosh(\nu x/L) - \cos(\nu x/L) - \gamma[\sinh(\nu x/L) - \sin(\nu x/L)]\} \tag{50}$$

where

$$\gamma = \frac{\cosh\nu + \cos\nu}{\sinh\nu + \sin\nu} \tag{51}$$

The simplified smart materials robot system (33–35) under conditions (47) can be solved if initial conditions are properly specified:

$$w(x,0) = w_0(x) \tag{52}$$

$$\dot{w}(x,0) = w_{0d}(x) \tag{53}$$

Letting $0 < \nu_1 < \nu_2 < \cdots < \infty$ be an infinite number of positive solutions to Eq. (46), we can obtain an infinite number of solutions to the boundary value problem, where $i = 1, 2, \ldots,$

$$\psi_i(x) = A_i\{\cosh(\nu_i x/L) - \cos(\nu_i x/L) - \gamma_i[\sinh(\nu_i x/L) - \sin(\nu_i x/L)]\} = A_i\bar{\psi}_i(x) \tag{54}$$

where the various γ_i are calculated by Eq. (46) with the corresponding ν_i, and the constants A_i are to be determinated later.

Because only case 1, Eq. (47), needs to be considered, constant k must be a positive scalar. Letting $k = \omega^2$ with ω being a positive number, Eq. (38) is now in the form

$$\ddot{Q}(t) + \omega^2 Q(t) = 0 \tag{55}$$

which indicates that $Q(t)$ is harmonic with frequency ω. Corresponding to the infinite number of ν_i, an infinite number of natural frequencies exist:

$$\omega_i = \frac{\nu_i^2}{L^2}\sqrt{\frac{c_L\beta_L - h_L^2}{\rho_L\beta_L}} \tag{56}$$

Subsequently, an infinite number of solutions to Eq. (55) can be obtained:

$$q_i(t) = B_i\cos\omega_i t + C_i\sin\omega_i t \tag{57}$$

where B_i and C_i are constants that will be determinated from the initial conditions later. Note that Eq. (33) is linear and homogeneous. From the superposition or linearity principles,[15] a solution $w(x, t)$ is given by

$$w(x,t) = \sum_{i=1}^{\infty}\psi_i(x)q_i(t) \tag{58}$$

The remaining problem is to determine A_i, B_i, and C_i. Before proceeding, the following orthogonal conditions are introduced:

$$\rho_L\int_0^L \psi_i\psi_j\,\mathrm{d}x + m_3\psi_i(L)\psi_j(L) = \begin{cases}0 & i\neq j\\ \rho_L & i=j\end{cases} \tag{59}$$

$$\frac{c_L\beta_L - h_L^2}{\beta_L}\int_0^L \psi_i''\psi_j''\,\mathrm{d}x = \begin{cases}0 & i\neq j\\ \omega_i^2\rho_L & i=j\end{cases} \tag{60}$$

By using these two orthogonal conditions, it can be found that

$$A_i = \left[\frac{1}{\int_0^L \bar\psi_i^2(x)\,\mathrm{d}x + (m_3/\rho_L)\bar\psi_i^2(L)}\right]^{\frac12} \tag{61}$$

$$B_i = \int_0^L w_0(x)\psi_i(x)\,\mathrm{d}x + \frac{m_3}{\rho_L}w_0(L)\psi_i(L) \tag{62}$$

$$C_i = \frac{1}{\omega_i}\left[\int_0^L w_{0d}(x)\psi_i(x)\,\mathrm{d}x + \frac{m_3}{\rho_L}w_{0d}(L)\psi_i(L)\right] \tag{63}$$

Moreover, from

$$\int_0^L \bar\psi_i^2(x)\,\mathrm{d}x = L$$

when $m_3 = 0$, A_i can be further calculated by

$$A_i = \begin{cases} L^{-\frac12} & m_3 = 0\\ \left[L + \dfrac{4m_3}{\rho_L}\left(\dfrac{\sinh\nu_i\cos\nu_i - \cosh\nu_i\sin\nu_i}{\sinh\nu_i + \sin\nu_i}\right)^2\right]^{-\frac12} & m_3 > 0\end{cases} \tag{64}$$

From Eqs. (34) and (58), the solution to the electrical displacement can be derived as

$$D_y(x,t) = \sum_{i=1}^{\infty} -\frac{h_L}{\beta_L}\psi_i''(x)q_i(t) \tag{65}$$

From Eq. (65), it can be seen that the electrical displacement is also the function of various $q_i(t)$, which means that the electrical dynamics with very high frequency have been neglected. It is reasonable because the frequencies of the mechanical vibration are far below those of the electrical vibration.

Note that the solutions of $w(x, t)$ and $D_y(x, t)$ obtained earlier are valid only for the conservative smart materials robot. For the original system (29–32), which is driven by torque τ and voltages V and thus is nonconservative, the solutions (58) and (65) are invalid. However, in the AMM modeling, the vibration of the nonconservative system is also assumed to be of the forms (58) and (65), except that the various $q_i(t)$, $i = 1, 2, \ldots$, are not given by Eq. (57) but depend on the torque τ and voltage V. In the context, the various $q_i(t)$, $i = 1, 2, \ldots$, are called the generalized coordinates of the system.

As stated earlier, in the AMM modeling, the elastic vibration of the smart materials robot is assumed to be of the form

$$w(x,t) = \sum_{i=0}^{\infty}\psi_i(x)q_i(t)$$

where the various $\psi_i(x)$ are given by Eq. (54) and the various $q_i(t)$ are the generalized coordinates. Each $q_i(t)$ corresponds to a degree of freedom of the system.

It is well known that the first several modes (corresponding to lower frequencies) are dominant in describing the system dynamics. The infinite series can be truncated into a finite one, i.e.,

$$w(x,t) = \sum_{i=0}^{N}\psi_i(x)q_i(t), \qquad 0\le x\le L \tag{66}$$

$$D_y(x,t) = \sum_{i=1}^{N} -\frac{h_L}{\beta_L}\psi_i''(x)q_i(t), \qquad 0\le x\le L \tag{67}$$

Define the generalized coordinates vector as

$$\boldsymbol{Q} := [\theta \quad q_1 \quad q_2 \quad \cdots \quad q_N]^T \in R^{N+1} \tag{68}$$

From Eqs. (7), (10), (11), (66), and (67) and considering the orthogonal conditions (59) and (60), the kinetic energy of the system is then given by

$$E_k = E_k^M + E_k^E = \tfrac12\dot{\boldsymbol{Q}}^T\boldsymbol{M}_A\dot{\boldsymbol{Q}} \tag{69}$$

where $\boldsymbol{M}_A \in R^{(N+1)\times(N+1)}$ is a symmetric and positive definite inertia matrix given by

$$\boldsymbol{M}_A = \begin{bmatrix} d & m_A^1 & m_A^2 & \cdots & m_A^N\\ m_A^1 & \sigma_A^1 & m_A^{12} & \cdots & m_A^{1N}\\ m_A^2 & m_A^{12} & \sigma_A^2 & \cdots & m_A^{2N}\\ \vdots & \vdots & \vdots & \vdots & \vdots\\ m_A^N & m_A^{1N} & m_A^{2N} & \cdots & \sigma_A^N\end{bmatrix} \tag{70}$$

with elements defined as follows:

$$d = I_h + I_p + I_b + \rho_L\sum_{i=1}^{N} q_i^2$$

with

$$I_b = \tfrac13\rho_L L^3, \qquad I_p = m_3L^2$$

$$\sigma_A^i = \rho_L + \frac{\mu_L h_L^2}{\beta_L^2}\int_0^L \psi_i'^2(x)\,\mathrm{d}x, \qquad i = 1, 2, \ldots \tag{71}$$

$$m_A^{ij} = \frac{\mu_L h_L^2}{\beta_L^2}\int_0^L \psi_i'(x)\psi_j'(x)\,\mathrm{d}x \qquad i, j = 1, 2, \ldots, \quad i\neq j$$

$$m_A^i = \rho_L\int_0^L x\psi_i(x)\,\mathrm{d}x + m_3L\psi_i(L), \qquad i = 1, 2, \ldots$$

Similarly, using Eqs. (12), (66), and (67), we can rewrite the potential energy of the system in the form

$$E_p = \tfrac12\boldsymbol{Q}^T\boldsymbol{K}_A\boldsymbol{Q} \tag{72}$$

where

$$\boldsymbol{K}_A = \mathrm{diag}\begin{bmatrix}0 & \omega_1^2\rho_L & \omega_2^2\rho_L & \cdots & \omega_N^2\rho_L\end{bmatrix} \in R^{(N+1)\times(N+1)} \tag{73}$$

The same process can be applied to the virtual work (15), and it can be rewritten as

$$\delta W = \boldsymbol{F}_A^T\delta\boldsymbol{Q} \tag{74}$$

where

$$\boldsymbol{F}_A = \left[\tau - \frac{bh_L}{\beta_L}\int_0^L V(x,t)\psi_1''(x)\,\mathrm{d}x - \frac{bh_L}{\beta_L}\int_0^L V(x,t)\psi_2''(x)\,\mathrm{d}x \cdots - \frac{bh_L}{\beta_L}\int_0^L V(x,t)\psi_N''(x)\,\mathrm{d}x\right]^T$$

The dynamic model of the smart materials robot can then be derived from the Euler–Lagrange equation

$$\frac{\mathrm{d}}{\mathrm{d}t}\frac{\partial L}{\partial \dot{\boldsymbol{Q}}} - \frac{\partial L}{\partial \boldsymbol{Q}} = \boldsymbol{T} \tag{75}$$

where $L = E_k - E_p$.

Substituting Eqs. (69), (72), and (74) into Euler–Lagrange equation (75) yields the dynamic model of the smart materials robot:

$$\boldsymbol{M}_A(\boldsymbol{Q})\ddot{\boldsymbol{Q}} + \boldsymbol{C}_A(\boldsymbol{Q},\dot{\boldsymbol{Q}})\dot{\boldsymbol{Q}} + \boldsymbol{K}_A\boldsymbol{Q} = \boldsymbol{F}_A \tag{76}$$

where the elements C_{A-kj} of $\boldsymbol{C}_A \in R^{(N+1)\times(N+1)}$ can be calculated by

$$C_{A-kj} = \sum_{i=0}^{N}\frac{1}{2}\left(\frac{\partial m_{A-kj}}{\partial q_i} + \frac{\partial m_{A-ki}}{\partial q_j} - \frac{\partial m_{A-ij}}{\partial q_k}\right)\dot{q}_i \tag{77}$$

with m_{A-ij} being the ijth element of matrix $\boldsymbol{M}_A$. Substituting m_{A-ij} just defined into Eq. (77), we obtain

$$\boldsymbol{C}_A = \begin{bmatrix} \rho_L\sum_{i=1}^{N} q_i\dot{q}_i & \rho_L q_1\dot{\theta} & \cdots & \rho_L q_N\dot{\theta} \\ -\rho_L q_1\dot{\theta} & & & \\ \vdots & & 0 & \\ -\rho_L q_N\dot{\theta} & & & \end{bmatrix} \tag{78}$$

It can be proven that $\dot{M}_A - 2C_A$ is skew symmetric. It can be seen that the AMM model of a smart materials robot is also different from the AMM model of a pure flexible robot, which can be derived from the AMM model of a smart materials robot by setting $h_L = 0$.

FEM Modeling

In this section, under the same assumptions as stated before, we derive the model of a smart materials robot by the FEM associated with the Lagrangian approach. According to the FEM, without losing generality, let the beam be divided into N parts with the same length $h = L/N$. Thus the system geometry changes into the form shown in Fig. 3.

Analysis of Finite Element

Assuming the deflection $w_i(x_i,t), 0 \le x_i \le h$ can be represented by a weighted sum of v_{ia}, ϕ_{ia}, v_{ib}, and ϕ_{ib}. In accordance with the boundary conditions, e.g., $w_i(0,t) = v_{ia}$, $\partial w_i(0,t)/\partial x = \phi_{ia}$, $w_i(h,t) = v_{ib}$, $\partial w_i(h,t)/\partial x = \phi_{ib}$, the weights can be chosen as third-order polynomials. Therefore, we have[15]

$$w_i(x_i) = \boldsymbol{P}_w^T(x_i)\boldsymbol{\alpha}_i \tag{79}$$

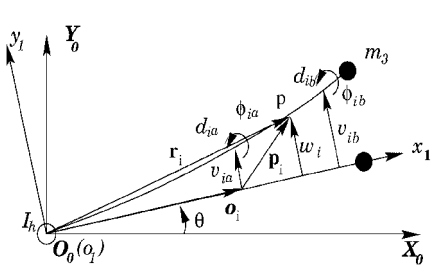

Fig. 3 Coordinate systems of the smart materials robot (FEM).

where

$$\boldsymbol{P}_w(x_i) = \begin{bmatrix} 1 - (3x_i^2/h^2) + (2x_i^3/h^3) \\ x_i - (2x_i^2/h) + (x_i^3/h^2) \\ (3x_i^2/h^2) - (2x_i^3/h^3) \\ -(x_i^2/h) + (x_i^3/h^2) \end{bmatrix}, \qquad \boldsymbol{\alpha}_i = \begin{bmatrix} v_{ia} \\ \phi_{ia} \\ v_{ib} \\ \phi_{ib} \end{bmatrix}$$

Moreover, the electrical displacement can also be expressed as

$$D_{y_i}(x_i) = \boldsymbol{P}_D^T(x_i)\boldsymbol{q}_{2i}$$
$$\boldsymbol{P}_D(x_i) = [1 - (x_i/h) \quad x_i/h]^T, \qquad \boldsymbol{q}_{2i} = [d_{ia} \quad d_{ib}]^T \tag{80}$$

For clarity, Maxwell equation (8) is rewritten here as

$$\nabla \times \boldsymbol{H} = \frac{\partial \boldsymbol{D}}{\partial t}$$

and we arrive at

$$H_{zi}(x_i) = \boldsymbol{P}_H^T(x_i)\dot{\boldsymbol{q}}_{2i} \tag{81}$$

where

$$\boldsymbol{P}_H(x_i) = \left[-x_i + (x_i^2/2h) \quad -x_i^2/2h\right]^T$$

From Eq. (81), it can be seen that the magnetic field intensity is related to the velocity of the coordinates. As a consequence, magnetic energy will be treated as electrical kinetic energy as before.[11]

Kinetic Energy

As stated earlier, kinetic energy includes both mechanical kinetic energy and so-called electrical kinetic energy, i.e., magnetic energy.

The position vector of point P in the ith element is given by

$$\boldsymbol{r}_i = \boldsymbol{o}_i + \boldsymbol{p}_i$$

where $\boldsymbol{o}_i$ and $\boldsymbol{p}_i$ are expressed in the fixed-base frame as follows:

$$\boldsymbol{o}_i = \boldsymbol{a}(\theta)\begin{bmatrix}(i-1)h \\ 0 \\ 0\end{bmatrix}, \qquad \boldsymbol{p}_i = \boldsymbol{a}(\theta)\begin{bmatrix}x_i \\ w_i(x_i) \\ 0\end{bmatrix}$$

with

$$\boldsymbol{a}(\theta) = \begin{bmatrix}\cos\theta & -\sin\theta & 0 \\ \sin\theta & \cos\theta & 0 \\ 0 & 0 & 1\end{bmatrix}$$

being the transfomation matrix from the local reference frame to the fixed-base frame. Thus the mechanical kinetic energy of the ith element is

$$E_{k,i}^M = \int_0^h \frac{1}{2}m(x_i)\dot{\boldsymbol{r}}_i^T\dot{\boldsymbol{r}}_i\,\mathrm{d}x_i = \frac{1}{2}\dot{\boldsymbol{q}}_{1i}^T \times \int_0^h m(x_i)\boldsymbol{a}_i^T(x_i,\boldsymbol{\alpha}_i)\boldsymbol{a}_i(x_i,\boldsymbol{\alpha}_i)\,\mathrm{d}x_i\,\dot{\boldsymbol{q}}_{1i} = \frac{1}{2}\dot{\boldsymbol{q}}_{1i}^T\boldsymbol{M}_i^M\dot{\boldsymbol{q}}_{1i} \tag{82}$$

where

$$\boldsymbol{a}_i(x_i,\boldsymbol{\alpha}_i) = \begin{bmatrix} -\boldsymbol{P}_w^T(x_i)\boldsymbol{\alpha}_i & 0 \\ [(i-1)h + x_i] & \boldsymbol{P}_w^T(x_i) \\ 0 & 0 \end{bmatrix}, \qquad \boldsymbol{q}_{1i} = \begin{bmatrix}\theta \\ \boldsymbol{\alpha}_i\end{bmatrix}$$

and $\boldsymbol{M}_i^M = m(x_i)\boldsymbol{N}_i^M$ with

$$m(x_i) = \begin{cases} ab\rho_1 + (c_1+c_2)b\rho_2, & i = 1,\ldots,(N-1) \\ ab\rho_1 + (c_1+c_2)b\rho_2 + m_3\delta(x_i - h), & i = N \end{cases}$$

being the mass per unit length and $\boldsymbol{N}_i^M$ being defined in the Appendix.

The electrical kinetic energy of the ith element is

$$E^E_{k,i} = \frac{1}{2}b\int_0^h \int_{-\frac{a}{2}-c_2}^{-\frac{a}{2}} [\boldsymbol{B}^T\boldsymbol{H}]\,\mathrm{d}y\,\mathrm{d}x_i + \frac{1}{2}b\int_0^h \int_{\frac{a}{2}}^{\frac{a}{2}+c_1} [\boldsymbol{B}^T\boldsymbol{H}]\,\mathrm{d}y\,\mathrm{d}x_i$$

$$= \frac{1}{2}\dot{\boldsymbol{q}}_{2i}^T \int_0^h \left[\mu_{33}b(c_1+c_2)\boldsymbol{P}_H(x_i)\boldsymbol{P}_H^T(x_i)\right]\mathrm{d}x_i\dot{\boldsymbol{q}}_{2i}$$

$$= \frac{1}{2}\dot{\boldsymbol{q}}_{2i}^T\boldsymbol{M}_i^E\dot{\boldsymbol{q}}_{2i} \tag{83}$$

where $\boldsymbol{M}_i^E = \mu_{33}b(c_1+c_2)\boldsymbol{N}_i^E$, with $\boldsymbol{N}_i^E$ being defined in the Appendix.

The total kinetic energy is then given by

$$E_{k,i} = E^M_{k,i} + E^E_{k,i} = \tfrac{1}{2}\dot{q}_{1i}^T\boldsymbol{M}_i^M\dot{q}_{1i} + \tfrac{1}{2}\dot{q}_{2i}^T\boldsymbol{M}_i^E\dot{q}_{2i} \tag{84}$$

Potential Energy

Potential energy includes three parts: the mechanical one, the electrical one, and the coupled one, which will be obtained as shown in Eq. (86).

The same as before, the strain is in order[13]

$$S_1 = -y\frac{\partial^2 w(x_i,t)}{\partial x_i^2} = -y\boldsymbol{P}_s^T(x_i)\boldsymbol{q}_{1i}$$

$$S_2 = S_3 = S_4 = S_5 = S_6 = 0$$

where

$$\boldsymbol{P}_s(x_i) = \left[0, -\frac{6}{h^2} + \frac{12x_i}{h^3}, -\frac{4}{h} + \frac{6x_i}{h^2}, \frac{6}{h^2} - \frac{12x_i}{h^3}, -\frac{2}{h} + \frac{6x_i}{h^2}\right]^T$$

The total potential energy for the ith element is then given by

$$E_{p,i} = \frac{1}{2}b\int_0^h \int_{-\frac{a}{2}-c_2}^{-\frac{a}{2}} [\boldsymbol{S}^T\boldsymbol{F}^S + \boldsymbol{E}^T\boldsymbol{D}]\,\mathrm{d}y\,\mathrm{d}x_i$$

$$+ \frac{1}{2}b\int_0^h \int_{-\frac{a}{2}}^{\frac{a}{2}} \boldsymbol{S}^T\boldsymbol{F}^M\,\mathrm{d}y\,\mathrm{d}x_i$$

$$+ \frac{1}{2}b\int_0^h \int_{\frac{a}{2}}^{\frac{a}{2}+c_1} [\boldsymbol{S}^T\boldsymbol{F}^S + \boldsymbol{E}^T\boldsymbol{D}]\,\mathrm{d}y\,\mathrm{d}x_i$$

$$= \frac{1}{2}\boldsymbol{q}_{1i}^T\int_0^h \left(\frac{1}{3}b\left[\frac{c_{11}^M a^3}{4} + c_{11}^S\left[\left(\frac{a}{2}+c_1\right)^3\right.\right.\right.$$

$$\left.\left.\left. + \left(\frac{a}{2}+c_2\right)^3 - \frac{a^3}{4}\right]\right| \boldsymbol{P}_s(x_i)\boldsymbol{P}_s^T(x_i)\right)\mathrm{d}x_i\boldsymbol{q}_{1i}$$

$$+ \frac{1}{2}\boldsymbol{q}_{2i}^T\int_0^h \left[(c_1+c_2)b\beta_{22}\boldsymbol{P}_D(x_i)\boldsymbol{P}_D^T(x_i)\right]\mathrm{d}x_i\boldsymbol{q}_{2i}$$

$$+ \boldsymbol{q}_{2i}^T\int_0^h \left[\tfrac{1}{2}h_{12}b(c_1-c_2)(c_1+c_2+a)\boldsymbol{P}_D(x_i)\boldsymbol{P}_s^T(x_i)\right]\mathrm{d}x_i\boldsymbol{q}_{1i}$$

$$= \frac{1}{2}\boldsymbol{q}_{1i}^T\boldsymbol{K}_i^M\boldsymbol{q}_{1i} + \frac{1}{2}\boldsymbol{q}_{2i}^T\boldsymbol{K}_i^E\boldsymbol{q}_{2i} + \boldsymbol{q}_{2i}^T\boldsymbol{K}_i^C\boldsymbol{q}_{1i} \tag{86}$$

where $\boldsymbol{K}_i^M = \frac{1}{3}b\{(c_{11}^m a^3/4) + c_{11}^s[(a/2)+c_1)^3 + (a/2+c_2)^3 - a^3/4]\}\boldsymbol{P}_i^M$, $\boldsymbol{K}_i^E = (c_1+c_2)b\beta_{22}\boldsymbol{P}_i^M$, and $\boldsymbol{K}_i^C = \frac{1}{2}h_{12}b(c_1-c_2)(c_1+c_2+a)\boldsymbol{P}_i^C$, with $\boldsymbol{P}_i^M$, $\boldsymbol{P}_i^E$, and $\boldsymbol{P}_i^C$ being defined in the Appendix.

Virtual Work

Similarly, virtual work also includes the mechanical one and the electrical one.

The mechanical virtual work done by the applied force is

$$\delta W_i^M = \int_0^h \tau_i(x_i,t)\delta\frac{\partial w_i(x_i,t)}{\partial x_i}\,\mathrm{d}x_i + \int_0^h \tau_i(x_i,t)\delta\theta\,\mathrm{d}x_i$$

where $\tau_i(x_i,t)$ is the motor torque applied to the ith element. Considering that there is only a motor torque $\tau(t)$ acting at the base, we obtain the mechanical virtual work as

$$\delta W_i^M = \delta\boldsymbol{q}_{1i}^T\boldsymbol{F}_i^M \tag{87}$$

where

$$\boldsymbol{F}_1^M = [\tau(t), 0, \tau(t), 0, 0]^T$$

$$\boldsymbol{F}_i^M = [0,0,0,0,0]^T, \qquad \text{for} \qquad i \neq 1$$

The electrical virtual work done by the voltage is

$$\delta W_i^E = \int_0^h bV_i(x_i,t)\delta D_i(x_i,t)\,\mathrm{d}x_i$$

Assuming that voltage $V_i(x_i,t)$ does not depend on x_i, we have

$$\delta W_i^E = \delta\boldsymbol{q}_{2i}^T\boldsymbol{F}_i^E \tag{88}$$

where

$$\boldsymbol{F}_i^E = [(bhV_i/2) \quad (bhV_i/2)]^T$$

Dynamic Equations

Applying the Euler–Lagrange equation (89), we can obtain the dynamic equation of the whole system:

$$\frac{\mathrm{d}}{\mathrm{d}t}\frac{\partial L}{\partial\dot{\boldsymbol{Q}}_{m,j}} - \frac{\partial L}{\partial\boldsymbol{Q}_{m,j}} = F_{m,j} \tag{89}$$

where $\boldsymbol{Q}_{m,j}$ are the components of the combination of vectors $\boldsymbol{q}_{1i}$ and $\boldsymbol{q}_{2i}$, $i = 1,\ldots,N$, which leads to the generalized coordinates

$$\boldsymbol{Q}_1 = [\theta, v_{1a}, \phi_{1a}, v_{2a}, \phi_{2a}, \ldots, v_{Na}, \phi_{Na}, v_{Nb}, \phi_{Nb}]^T$$

$$\boldsymbol{Q}_2 = [d_{1a}, d_{2a}, \ldots, d_{Na}, d_{Nb}]^T$$

$$L = \sum_{i=1}^{i=N}[E_{k,i} - E_{p,i}] = \sum_{i=1}^{i=N}\left[\frac{1}{2}\left(\dot{\boldsymbol{q}}_{1i}^T\boldsymbol{M}_i^M\dot{\boldsymbol{q}}_{1i} + \dot{\boldsymbol{q}}_{2i}^T\boldsymbol{M}_i^E\dot{\boldsymbol{q}}_{2i}\right)\right.$$

$$\left. - \left(\frac{1}{2}\boldsymbol{q}_{1i}^T\boldsymbol{K}_i^M\boldsymbol{q}_{1i} + \frac{1}{2}\boldsymbol{q}_{2i}^T\boldsymbol{K}_i^E\boldsymbol{q}_{2i}\right) - \boldsymbol{q}_{2i}^T\boldsymbol{K}_i^C\boldsymbol{q}_{1i}\right]$$

$$= \frac{1}{2}\dot{\boldsymbol{Q}}_1^T\boldsymbol{M}^M\dot{\boldsymbol{Q}}_1 + \frac{1}{2}\dot{\boldsymbol{Q}}_2^T\boldsymbol{M}^E\dot{\boldsymbol{Q}}_2$$

$$- \left(\frac{1}{2}\boldsymbol{Q}_1^T\boldsymbol{K}^M\boldsymbol{Q}_1 + \frac{1}{2}\boldsymbol{Q}_2^T\boldsymbol{K}^E\boldsymbol{Q}_2\right) - \frac{1}{2}\boldsymbol{Q}_2^T\boldsymbol{K}^C\boldsymbol{Q}_1 \tag{90}$$

and

$$\boldsymbol{F}_1^T\delta\boldsymbol{Q}_1 = \sum_{i=1}^{i=N}\delta\boldsymbol{q}_{1i}^T\boldsymbol{F}_i^M = \left(\sum_{i=1}^{i=N}\boldsymbol{F}_{i,\text{ext}}^M\right)^T\delta\boldsymbol{Q}_1$$

$$\boldsymbol{F}_2^T\delta\boldsymbol{Q}_2 = \sum_{i=1}^{i=N}\delta\boldsymbol{q}_{2i}^T\boldsymbol{F}_i^E = \left(\sum_{i=1}^{i=N}\boldsymbol{F}_{i,\text{ext}}^E\right)^T\delta\boldsymbol{Q}_2 \tag{91}$$

$$\boldsymbol{M}^M = \sum_{i=1}^{i=N}\boldsymbol{M}_{i,\text{ext}}^M, \qquad \boldsymbol{M}^E = \sum_{i=1}^{i=N}\boldsymbol{M}_{i,\text{ext}}^E, \qquad \boldsymbol{K}^M = \sum_{i=1}^{i=N}\boldsymbol{K}_{i,\text{ext}}^M$$

$$\boldsymbol{K}^E = \sum_{i=1}^{i=N}\boldsymbol{K}_{i,\text{ext}}^E, \qquad \boldsymbol{K}^C = \sum_{i=1}^{i=N}\boldsymbol{K}_{i,\text{ext}}^C \tag{92}$$

with $*_{i,\text{ext}}$ being the extended form of matrix $*_i$ in accordance with $\boldsymbol{Q}_1$ and $\boldsymbol{Q}_2$, whereas $*_i$ is in accordance with $\boldsymbol{q}_{1i}$ and $\boldsymbol{q}_{2i}$. The term I_h is added to $\boldsymbol{M}_{1,11}^M$ to include the kinetic energy of the hub, i.e., $\frac{1}{2}I_h\dot{\theta}^2$. With regard to the boundary conditions, $v_{1a} = 0$, $\phi_{1a} = 0$, corresponding rows and/or columns of extended matrices should be removed.

Subsequently, the dynamic equations of the whole system are given by

$$\boldsymbol{M}^M\ddot{\boldsymbol{Q}}_1 + \boldsymbol{C}^M(\boldsymbol{Q}_1, \dot{\boldsymbol{Q}}_1)\dot{\boldsymbol{Q}}_1 + \boldsymbol{K}^M\boldsymbol{Q}_1 + \boldsymbol{K}^{C^T}\boldsymbol{Q}_2 = \boldsymbol{F}_1 \tag{93}$$

$$\boldsymbol{M}^E\ddot{\boldsymbol{Q}}_2 + \boldsymbol{K}^E\boldsymbol{Q}_2 + \boldsymbol{K}^C\boldsymbol{Q}_1 = \boldsymbol{F}_2 \tag{94}$$

Note that $Q_{1,2}$ and $Q_{1,3}$ have been removed from the vector $\boldsymbol{Q}_1$; correspondingly,the coefficient matrices' rows and/or columns that are related to coordinates $Q_{1,2}$ and $Q_{1,3}$ are also removed. The jkth elements of the centripetal/Coriolis matrix $\boldsymbol{C}^M$ have the following form:

$$C^M_{jk} = \frac{1}{2}\sum_{l=1}^{l=N}\left[\frac{\partial M^M_{jk}}{\partial Q_{1,l}} + \frac{\partial M^M_{jl}}{\partial Q_{1,k}} - \frac{\partial M^M_{kl}}{\partial Q_{1,j}}\right]\dot{Q}_{1,l}$$

If we further define $\boldsymbol{Q} = \begin{bmatrix}\boldsymbol{Q}_1^T & \boldsymbol{Q}_2^T\end{bmatrix}^T$, Eqs. (93) and (94) can be combined into

$$\boldsymbol{M}\ddot{\boldsymbol{Q}} + \boldsymbol{C}(\boldsymbol{Q}, \dot{\boldsymbol{Q}})\dot{\boldsymbol{Q}} + \boldsymbol{K}\boldsymbol{Q} = \boldsymbol{F} \tag{95}$$

where

$$\boldsymbol{M} = \begin{bmatrix}\boldsymbol{M}^M & 0\\ 0 & \boldsymbol{M}^E\end{bmatrix}, \qquad \boldsymbol{C} = \begin{bmatrix}\boldsymbol{C}^M & 0\\ 0 & 0\end{bmatrix}$$

$$\boldsymbol{K} = \begin{bmatrix}\boldsymbol{K}^M & \boldsymbol{K}^{C^T}\\ \boldsymbol{K}^C & \boldsymbol{K}^E\end{bmatrix}, \qquad \boldsymbol{F} = \begin{bmatrix}\boldsymbol{F}_1\\ \boldsymbol{F}_2\end{bmatrix}$$

This model will be referred to as the full FEM model in the later discussion.

Because matrix $\boldsymbol{M}^E$ in Eq. (94) is very small, dynamics equation (94) is usually omitted. Thus a reduced system is obtained:

$$\boldsymbol{M}^M\ddot{\boldsymbol{Q}}_1 + \boldsymbol{C}^M(\boldsymbol{Q}_1, \dot{\boldsymbol{Q}}_1)\dot{\boldsymbol{Q}}_1 + \left(\boldsymbol{K}^M - \boldsymbol{K}^{C^T}\boldsymbol{K}^{E^{-1}}\boldsymbol{K}^C\right)\boldsymbol{Q}_1 = \boldsymbol{F}_1 - \boldsymbol{K}^{C^T}\boldsymbol{K}^{E^{-1}}\boldsymbol{F}_2 \tag{96}$$

This model can also be derived by removing the electrical kinetic energy from the system kinetic energy. It will be referred to as the reduced FEM model in the following discussion.

We have the following remarks on the system properties, which are similar to those of the pure flexible robot.[4]

1) The matrix $\boldsymbol{M}$ is symmetric and positive definite.

2) The matrix $\frac{1}{2}\dot{\boldsymbol{M}} - \boldsymbol{C}(\boldsymbol{Q}, \dot{\boldsymbol{Q}})$ is skew symmetric.

3) Although $\boldsymbol{K}^M$ and $\boldsymbol{K}^E$ are semipositive definite, $\boldsymbol{K}$ in the full FEM model and $\boldsymbol{K}^M - \boldsymbol{K}^{C^T}\boldsymbol{K}^{E^{-1}}\boldsymbol{K}^C$ in the reduced FEM model can be nonpositive definite if the value or structure of $\boldsymbol{K}^C$ changes.

Remark 3 is in compliance with the results of the AMM modeling. It shows that the open-loop system may be unstable for certain system parameters. Note that, although the first two properties are similar to those of a pure flexible robot, the third property is quite different from that of a pure flexible robot.

Open-Loop Simulation

We will take the open-loop simulations of both the AMM model and the FEM model and compare them with each other. The system parameters are listed in Table 1.

Figures 4 and 5 show the tip deflection of the system when no voltages are applied and a torque 0.1 Nm is applied on the hub for 0.1 s. Figure 4 shows that the responses become close to each other as the number of the mode in the AMM model increases. It verifies that the dynamics of a smart materials robot is determined by the dominant modes with lower frequencies. From Fig. 5, it is easy to see that the responses of the AMM model and the FEM model become closer to each other as the number of elements of the FEM model increases. These figures verify the correctness of both models.

When the frequency responses are investigated, two cases are checked. First, we use the torque as the input and the joint angle and the tip deflection as the outputs. Second, the voltage at the base is used as the input, and the outputs are the same as in the first case. If voltages are applied at other points of the beam, the frequency responses can be similarly obtained.

Table 1 System parameters

Names	Values
I, kgm^2	0.05
a, m	0.008
c_1, m	0.008
c_2, m	0.004
b, m	0.01
ρ_1, kg/m^3	500
ρ_2, kg/m^3	500
m_3, kg	0
L, m	1
c^m_{11}, N/m^2	3×10^8
c^s_{11}, N/m^2	3×10^8
μ, H/m	1.2×10^{-6}
β, m/F	4×10^{12}
h, V/m	1×10^9

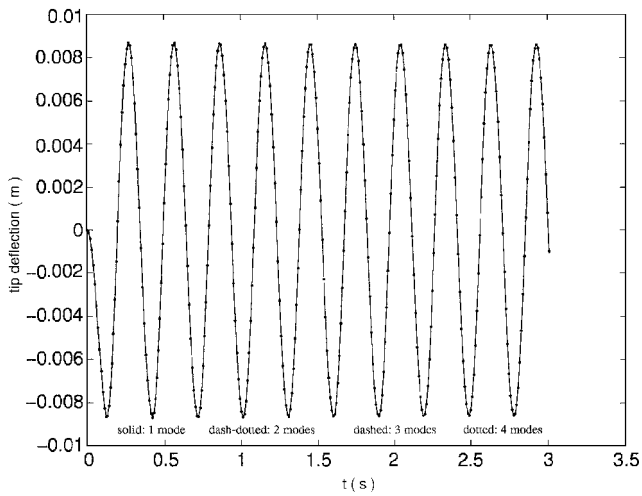

Fig. 4 Tip deflections of smart materials robot with different numbers of modes.

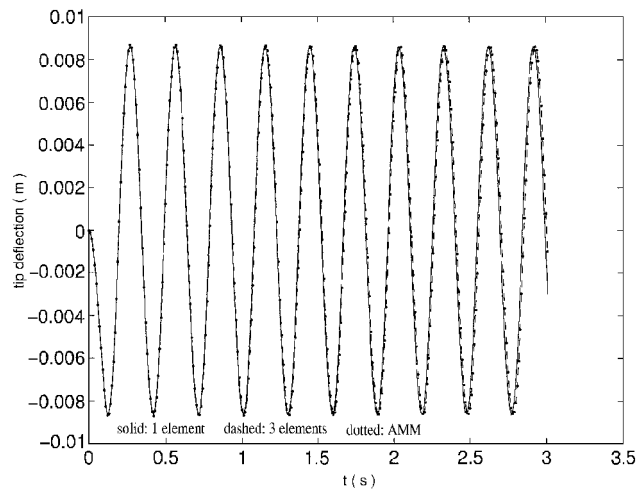

Fig. 5 Tip deflections of smart materials robot.

When only the torque is used as the input, from the frequency responses shown in Figs. 6 and 7. we can see that the response of the AMM model and that of the FEM model are very close to each other in the low-frequency ranges. In Fig. 6, from the resonant vibration peaks, it can be seen that strong couplings of the first two flexible modes, which are of lower frequencies, exist, whereas the couplings with higher-frequency modes are too weak to be seen and thus can be omitted in practice. From the frequency response in Fig. 7, it can also be clearly seen that the electrical dynamics with high frequencies are so strongly damped that they can be omitted. This is in line with the theoretical results derived in the preceding sections of AMM modeling and FEM modeling.

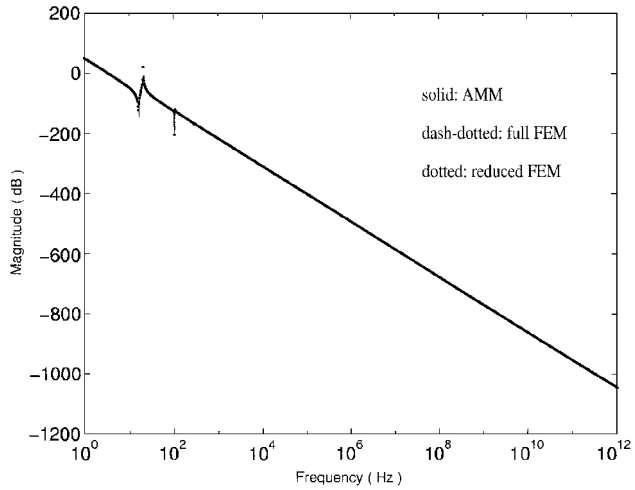

Fig. 6 Frequency response with torque as input and angle as output.

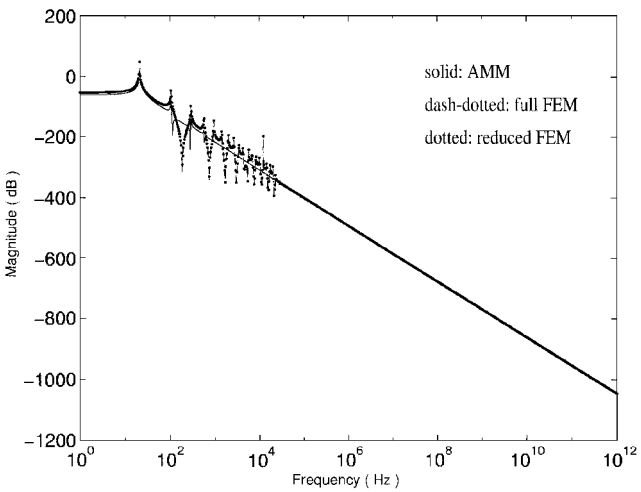

Fig. 7 Frequency response with torque as input and tip deflection as output.

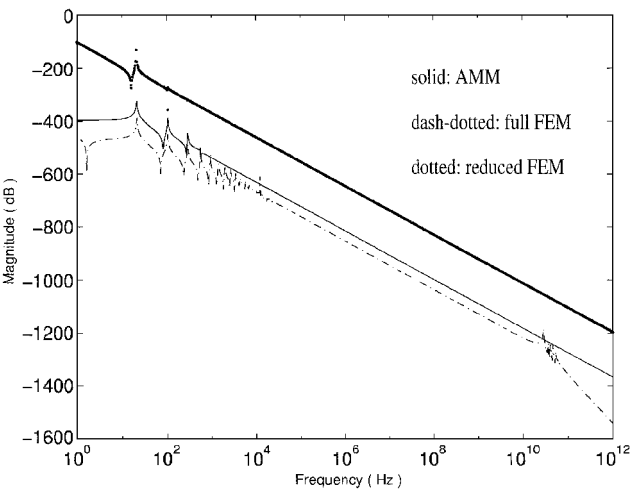

Fig. 8 Frequency response with voltage as input and angle as output.

When only the base voltage is used as input, it can be seen that differences exist in Figs. 8 and 9. This is reasonable because we treated electrical parts of the system differently in the three models. In the AMM model, both the electrical displacements and the mechanical deflections are functions of the same generalized coordinates as described in Eqs. (66) and (67), and electrical kinetic energy is included in Eq. (69). In the full FEM model, both electrical dynamics and the electrical kinetic energy are considered. In the reduced FEM model, because $\boldsymbol{M}^E$ is very small, the electrical dynamics is ignored, and the electrical kinetic energy is omitted as shown in Eq. (96). Therefore, in Figs. 8 and 9, there are resonant vibration peaks in the high-frequency range (10^{10}–10^{12} Hz) for the full FEM model, whereas there are no such peaks for the AMM model and the reduced FEM model. From Figs. 8 and 9, it can be seen that the electrical dynamics is strongly damped (from −100 dB in the low-frequency range to more than −1000 dB in the high-frequency range) in all cases; therefore, all of the models can be used in practice for different applications.

For a one-element system, the eigenvalues of item $\boldsymbol{K}$ in Eq. (95) and those of the item $\boldsymbol{K}^M - \boldsymbol{K}^{C^T}\boldsymbol{K}^{E^{-1}}\boldsymbol{K}^C$ in Eq. (96) are listed in Tables 2 and 3. We found that some eigenvalues become negative when h_{12} becomes sufficient large and results in an unstable system. The results verify Remark 3 stated in the preceding section.

Table 2 Eigenvalues of $\boldsymbol{K}$

$h, V/m$	Eigenvalues
10^9	1.7669
	34.0678
	0.8×10^8
	2.4×10^8
10^{10}	1.7408
	33.5658
	0.8×10^8
	2.4×10^8
10^{11}	−0.8625
	−16.631
	0.8×10^8
	2.4×10^8
10^{12}	−261.119
	−5035.97
	0.8×10^8
	2.4×10^8

Table 3 Eigenvalues of $\boldsymbol{K}^M - \boldsymbol{K}^{C^T}\boldsymbol{K}^{E^{-1}}\boldsymbol{K}^C$

$h, V/m$	Eigenvalues
10^9	1.7669
	34.0678
10^{10}	1.7408
	33.5658
10^{11}	−0.8625
	−16.631
10^{12}	−261.119
	−5036.29

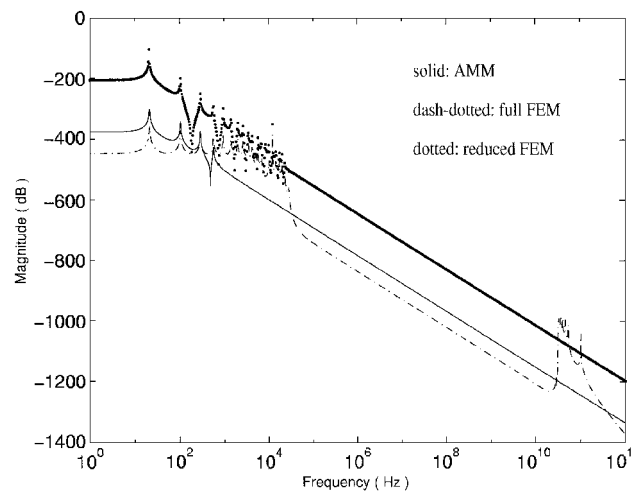

Fig. 9 Frequency response with voltage as input and tip deflection as output.

Conclusion

Three dynamic models of a smart materials robot have been derived in this paper. Although the infinite dimensional Hamilton model is too complicated to be applicable in engineering practice, it is the foundation to understand the properties of this system and to derive the AMM model and the FEM model, which have been truncated into finite dimensional form. Both the AMM model and the FEM model can be used in the controller design, whereas the generalized coordinates in the FEM model are more physically meaningful than those in the AMM model. All of these models have shown that the model of a smart materials robot cannot be simply taken to be the same as that of a pure flexible robot. The electrical dynamics and mechanical dynamics have been included in the full models, and the systemic analyses and frequency responses have shown that the former dynamics can be omitted in engineering applications. Both mathematical models and numerical simulations have shown that the stability of the open-loop system depends on the parameter and the structure of the smart materials robot.

Appendix: Entries of Matrices N_i^M, N_i^E, P_i^M, P_i^E, and P_i^C

$$N_{i,11}^M = n_1 v_{ia}^2 + n_2 \phi_{ia}^2 + n_3 v_{ib}^2 + n_4 \phi_{ib}^2 + 2n_5 v_{ia}\phi_{ia} + 2n_6 v_{ia} v_{ib} + 2n_7 v_{ia}\phi_{ib} + 2n_8 \phi_{ia} v_{ib} + 2n_9 \phi_{ia}\phi_{ib} + 2n_{10} v_{ib}\phi_{ib} + n_{11}$$

$$N_{i,12}^M = N_{i,21}^M = \left[(i-1)hx_i + \frac{1}{2}x_i^2 + \frac{(1-i)}{h}x_i^3 + \frac{2i-5}{4h^2}x_i^4 + \frac{2}{5h^3}x_i^5\right]\Bigg|_{x_i=0}^{h} = \left(\frac{i}{2} - \frac{7}{20}\right)h^2$$

$$N_{i,13}^M = N_{i,31}^M = \left[\frac{(i-1)h}{2}x_i^2 + \frac{3-2i}{3}x_i^3 + \frac{(i-3)x_i^4}{4h} + \frac{x^5}{5h^2}\right]\Bigg|_{x_i=0}^{h} = \left(\frac{i}{12} - \frac{1}{20}\right)h^3$$

$$N_{i,14}^M = N_{i,41}^M = \left[\frac{(i-1)x_i^3}{h} + \frac{(5-2i)x_i^4}{4h^2} - \frac{2x_i^5}{5h^3}\right]\Bigg|_{x_i=0}^{h} = \left(\frac{i}{2} - \frac{3}{20}\right)h^2$$

$$N_{i,15}^M = N_{i,51}^M = \left[\frac{(1-i)x_i^3}{3} + \frac{(i-2)x_i^4}{4h} + \frac{x_i^5}{5h^2}\right]\Bigg|_{x_i=0}^{h} = \left(-\frac{i}{12} + \frac{1}{30}\right)h^3$$

$$N_{i,22}^M = n_1, \qquad N_{i,23}^M = N_{i,32}^M = n_5$$

$$N_{i,24}^M = N_{i,42}^M = n_6, \qquad N_{i,25}^M = N_{i,52}^M = n_7$$

$$N_{i,33}^M = n_2, \qquad N_{i,34}^M = N_{i,43}^M = n_8$$

$$N_{i,35}^M = N_{i,53}^M = n_9, \qquad N_{i,44}^M = n_3$$

$$N_{i,45}^M = N_{i,54}^M = n_{10}, \qquad N_{i,55}^M = n_4$$

where

$$n_1 = \left[x_i - \frac{2x_i^3}{h^2} + \frac{x_i^4}{h^3} + \frac{9x_i^5}{5h^4} - \frac{2x_i^6}{h^5} + \frac{4x_i^7}{7h^6}\right]\Bigg|_{x_i=0}^{h} = \frac{13}{35}h$$

$$n_2 = \left[\frac{x_i^3}{3} - \frac{x_i^4}{h} + \frac{6x_i^5}{5h^2} - \frac{2x_i^6}{3h^3} + \frac{x_i^7}{7h^4}\right]\Bigg|_{x_i=0}^{h} = \frac{1}{105}h^3$$

$$n_3 = \left[\frac{9x_i^5}{5h^4} - \frac{2x_i^6}{h^5} + \frac{4x_i^7}{7h^6}\right]\Bigg|_{x_i=0}^{h} = \frac{13}{35}h$$

$$n_4 = \left[\frac{x_i^5}{5h^2} - \frac{x_i^6}{3h^3} + \frac{x_i^7}{7h^4}\right]\Bigg|_{x_i=0}^{h} = \frac{1}{105}h^3$$

$$n_5 = \left[\frac{1}{2}x_i^2 - \frac{2x_i^3}{3h} - \frac{x_i^4}{2h^2} + \frac{8x_i^5}{5h^3} - \frac{7x_i^6}{6h^4} + \frac{2x_i^7}{7h^5}\right]\Bigg|_{x_i=0}^{h} = \frac{11}{210}h^2$$

$$n_6 = \left[\frac{x_i^3}{h^2} - \frac{x_i^4}{2h^3} - \frac{9x_i^5}{5h^4} + \frac{2x_i^6}{h^5} - \frac{4x_i^7}{7h^6}\right]\Bigg|_{x_i=0}^{h} = \frac{9}{70}h$$

$$n_7 = \left[-\frac{x_i^3}{3h} + \frac{x_i^4}{4h^2} + \frac{3x_i^5}{5h^3} - \frac{5x_i^6}{6h^4} + \frac{2x_i^7}{7h^5}\right]\Bigg|_{x_i=0}^{h} = -\frac{13}{420}h^2$$

$$n_8 = \left[\frac{3x_i^4}{4h^2} - \frac{8x_i^5}{5h^3} + \frac{7x_i^6}{6h^4} - \frac{2x_i^7}{7h^5}\right]\Bigg|_{x_i=0}^{h} = \frac{13}{420}h^2$$

$$n_9 = \left[-\frac{x_i^4}{4h} + \frac{3x_i^5}{5h^2} - \frac{x_i^6}{2h^3} + \frac{x_i^7}{7h^4}\right]\Bigg|_{x_i=0}^{h} = -\frac{1}{140}h^3$$

$$n_{10} = \left[-\frac{3x_i^5}{5h^3} + \frac{5x_i^6}{6h^4} - \frac{2x_i^7}{7h^5}\right]\Bigg|_{x_i=0}^{h} = -\frac{11}{210}h^2$$

$$n_{11} = \left[(i-1)^2h^2x_i + (i-1)hx_i^2 + \frac{x_i^3}{3}\right]$$

$$N_{i,11}^E = \int_0^h \left[x_i^2 - \frac{x_i^3}{h} + \frac{x_i^4}{4h^2}\right]dx_i = \left[\frac{x_i^3}{3} - \frac{x_i^4}{4h} + \frac{x_i^5}{20h^2}\right]\Bigg|_{x_i=0}^{x_i=h} = \frac{2}{15}h^3$$

$$N_{i,12}^E = N_{i,21}^E = \int_0^h \left[\frac{x_i^3}{2h} - \frac{x_i^4}{4h^2}\right]dx_i = \left[\frac{x_i^4}{8h} - \frac{x_i^5}{20h^2}\right]\Bigg|_{x_i=0}^{x_i=h} = \frac{3}{40}h^3$$

$$N_{i,22}^E = \int_0^h \frac{x_i^4}{4h^2}\,dx_i = \frac{x_i^5}{20h^2}\Bigg|_{x_i=0}^{x_i=h} = \frac{1}{20}h^3$$

$$P_{i,22}^M = \int_0^h \left[\frac{36}{h^4} - \frac{144x_i}{h^5} + \frac{144x_i^2}{h^6}\right]dx_i = \left[\frac{36x_i}{h^4} - \frac{72x_i^2}{h^5} + \frac{48x_i^3}{h^6}\right]\Bigg|_{x_i=0}^{h} = \frac{12}{h^3}$$

$$P_{i,23}^M = Pb_{i,32}^M = \int_0^h \left[\frac{24}{h^3} - \frac{84x_i}{h^4} + \frac{72x_i^2}{h^5}\right]dx_i = \left[\frac{24x_i}{h^3} - \frac{42x_i^2}{h^4} + \frac{24x_i^3}{h^5}\right]\Bigg|_{x_i=0}^{h} = \frac{6}{h^2}$$

$$P^M_{i,24} = P^M_{i,42} = \int_0^h \left[-\frac{36}{h^4} + \frac{144x_i}{h^5} - \frac{144x_i^2}{h^6}\right] \mathrm{d}x_i$$

$$= \left[-\frac{36x_i}{h^4} + \frac{72x_i^2}{h^5} - \frac{48x_i^3}{h^6}\right]\Bigg|_{x_i=0}^{h} = -\frac{12}{h^3}$$

$$P^M_{i,25} = P^M_{i,52} = \int_0^h \left[\frac{12}{h^3} - \frac{60x_i}{h^4} + \frac{72x_i^2}{h^5}\right] \mathrm{d}x_i$$

$$= \left[\frac{12x_i}{h^3} - \frac{30x_i^2}{h^4} + \frac{24x_i^3}{h^5}\right]\Bigg|_{x_i=0}^{h} = \frac{6}{h^2}$$

$$P^M_{i,33} = \int_0^h \left[\frac{16}{h^2} - \frac{48x_i}{h^3} + \frac{36x_i^2}{h^4}\right] \mathrm{d}x_i$$

$$= \left[\frac{16x_i}{h^2} - \frac{24x_i^2}{h^3} + \frac{12x_i^3}{h^5}\right]\Bigg|_{x_i=0}^{h} = \frac{4}{h}$$

$$P^M_{i,34} = P^M_{i,43} = \int_0^h \left[-\frac{24}{h^3} + \frac{84x_i}{h^4} - \frac{72x_i^2}{h^5}\right] \mathrm{d}x_i$$

$$= \left[-\frac{24x_i}{h^3} + \frac{42x_i^2}{h^4} - \frac{24x_i^3}{h^5}\right]\Bigg|_{x_i=0}^{h} = -\frac{6}{h^2}$$

$$P^M_{i,35} = P^M_{i,53} = \int_0^h \left[\frac{8}{h^2} - \frac{36x_i}{h^3} + \frac{36x_i^2}{h^4}\right] \mathrm{d}x_i$$

$$= \left[\frac{8x_i}{h^2} - \frac{18x_i^2}{h^3} + \frac{12x_i^3}{h^4}\right]\Bigg|_{x_i=0}^{h} = \frac{2}{h}$$

$$P^M_{i,44} = \int_0^h \left[\frac{36}{h^4} - \frac{144x_i}{h^5} + \frac{144x_i^2}{h^6}\right] \mathrm{d}x_i$$

$$= \left[\frac{36x_i}{h^4} - \frac{72x_i^2}{h^5} + \frac{48x_i^3}{h^6}\right]\Bigg|_{x_i=0}^{h} = \frac{12}{h^3}$$

$$P^M_{i,45} = P^M_{i,54} = \int_0^h \left[-\frac{12}{h^3} + \frac{60x_i}{h^4} - \frac{72x_i^2}{h^5}\right] \mathrm{d}x_i$$

$$= \left[-\frac{12x_i}{h^3} + \frac{30x_i^2}{h^4} - \frac{24x_i^3}{h^5}\right]\Bigg|_{x_i=0}^{h} = -\frac{6}{h^2}$$

$$P^M_{i,55} = \int_0^h \left[\frac{4}{h^2} - \frac{24x_i}{h^3} + \frac{36x_i^2}{h^4}\right] \mathrm{d}x_i$$

$$= \left[\frac{4x_i}{h^2} - \frac{12x_i^2}{h^3} + \frac{12x_i^3}{h^4}\right]\Bigg|_{x_i=0}^{h} = \frac{4}{h}$$

$$P^M_{i,1j} = P^M_{i,j1} = 0, \qquad j = 1, 2, \ldots, 5$$

$$P^E_{i,11} = \int_0^h \left[1 - \frac{2x_i}{h} + \frac{x_i^2}{h^2}\right] \mathrm{d}x_i = \left[x_i - \frac{x_i^2}{h} + \frac{x_i^3}{3h^2}\right]\Bigg|_{x_i=0}^{h} = \frac{h}{3}$$

$$P^E_{i,12} = P^E_{i,21} = \int_0^h \left[\frac{x_i}{h} - \frac{x_i^2}{h^2}\right] \mathrm{d}x_i = \left[\frac{x_i^2}{2h} - \frac{x_i^3}{3h^2}\right]\Bigg|_{x_i=0}^{h} = \frac{h}{6}$$

$$P^E_{i,22} = \int_0^h \frac{x_i^2}{h^2} \mathrm{d}x_i = \frac{x_i^3}{3h^2}\Bigg|_{x_i=0}^{h} = \frac{h}{3}$$

$$P^C_{i,11} = 0$$

$$P^C_{i,12} = \int_0^h \left[-\frac{6}{h^2} + \frac{18x_i}{h^3} - \frac{12x_i^2}{h^4}\right] \mathrm{d}x_i$$

$$= \left[-\frac{6x_i}{h^2} + \frac{9x_i^2}{h^3} - \frac{4x_i^3}{h^4}\right]\Bigg|_{0}^{h} = -\frac{1}{h}$$

$$P^C_{i,13} = \int_0^h \left[-\frac{4}{h} + \frac{10x_i}{h^2} - \frac{6x_i^2}{h^3}\right] \mathrm{d}x_i$$

$$= \left[-\frac{4x_i}{h} + \frac{5x_i^2}{h^2} - \frac{2x_i^3}{h^3}\right]\Bigg|_{0}^{h} = -1$$

$$P^C_{i,14} = \int_0^h \left[\frac{6}{h^2} - \frac{18x_i}{h^3} + \frac{12x_i^2}{h^4}\right] \mathrm{d}x_i = \left[\frac{6x_i}{h^2} - \frac{9x_i^2}{h^3} + \frac{4x_i^3}{h^4}\right]\Bigg|_{0}^{h} = \frac{1}{h}$$

$$P^C_{i,15} = \int_0^h \left[-\frac{2}{h} + \frac{8x_i}{h^2} - \frac{6x_i^2}{h^3}\right] \mathrm{d}x_i = \left[-\frac{2x_i}{h} + \frac{4x_i^2}{h^2} - \frac{2x_i^3}{h^3}\right]\Bigg|_{0}^{h} = 0$$

$$P^C_{i,21} = 0$$

$$P^C_{i,22} = \int_0^h \left[-\frac{6x_i}{h^3} + \frac{12x_i^2}{h^4}\right] \mathrm{d}x_i = \left[-\frac{3x_i^2}{h^3} + \frac{4x_i^3}{h^4}\right]\Bigg|_{0}^{h} = \frac{1}{h}$$

$$P^C_{i,23} = \int_0^h \left[-\frac{4x_i}{h^2} + \frac{6x_i^2}{h^3}\right] \mathrm{d}x_i = \left[-\frac{2x_i^2}{h^2} + \frac{2x_i^3}{h^3}\right]\Bigg|_{0}^{h} = 0$$

$$P^C_{i,24} = \int_0^h \left[\frac{6x_i}{h^3} - \frac{12x_i^2}{h^4}\right] \mathrm{d}x_i = \left[\frac{3x_i^2}{h^3} - \frac{4x_i^3}{h^4}\right]\Bigg|_{0}^{h} = -\frac{1}{h}$$

$$P^C_{i,25} = \int_0^h \left[-\frac{2x_i}{h^2} + \frac{6x_i^2}{h^3}\right] \mathrm{d}x_i = \left[-\frac{x_i^2}{h^2} + \frac{2x_i^3}{h^3}\right]\Bigg|_{0}^{h} = 1$$

References

[1] Ge, S. S., Lee, T. H., and Zhu, G., "Asymptotically Stable End-Point Regulation of a Flexible SCARA/Cartesian Robot," *IEEE/ASME Transactions on Mechatronics*, Vol. 3, No. 2, 1998, pp. 138–144.

[2] Ge, S. S., Lee, T. H., and Zhu, G., "Genetic Algorithm Tuning of Lyapunov-Based Controllers: An Application to a Single-Link Flexible Robot System," *IEEE Transactions on Industrial Electronics*, Vol. 43, No. 5, 1996, pp. 567–674.

[3] Ge, S. S., Lee, T. H., and Zhu, G., "Improving Regulation of a Single-Link Flexible Manipulator with Strain Feedback," *IEEE Transactions on Robotics and Automation*, Vol. 14, No. 1, 1998, pp. 179–185.

[4] Ge, S. S., Lee, T. H., and Zhu, G., "A Nonlinear Feedback Controller for a Single-Link Flexible Manipulator Based on a Finite Element Model," *Journal of Robotic Systems*, Vol. 14, No. 3, 1997, pp. 165–178.

[5] Hagood, N. W., Chung, W. H., and Flotow, A. V., "Modelling of Piezoelectric Actuator Dynamics for Active Structural Control," *Journal of Intelligent Systems and Structures*, Vol. 1, No. 3, 1990, pp. 327–355.

[6] Crawley, E. F., and Luis, J., "Use of Piezoelectric Actuators as Elements of Intelligent Structures," *AIAA Journal*, Vol. 25, No. 10, 1987, pp. 1373–1385.

[7] Baily, T., and Hubbard, J. E., "Distributed Piezoelectric-Polymer Active Vibration Control of a Cantilever Beam," *Journal of Guidance, Control, and Dynamics*, Vol. 8, No. 5, 1985, pp. 605–611.

[8]Cundari, M., and Abedian, B., "The Dynamic Behavior of a Polyvinylidene Fluoride Piezoelectric Motional Device," *Smart Structures and Materials*, AD-Vol. 24/AMD-Vol. 123, American Society of Mechanical Engineers, New York, 1991, pp. 25–31.

[9]Yang, S. M., and Lee, Y. J., "Interaction of Structure Vibration and Piezoelectric Actuation," *Smart Materials and Structures*, Vol. 3, No. 4, 1994, pp. 494–500.

[10]Ikeda, T., *Fundamentals of Piezoelectricity*, Oxford Science Publications, Oxford, England, UK, 1990, Chap. 2.

[11]Hammond, P., *Energy Methods in Electromagnetism*, Clarendon, Oxford, England, UK, 1981, Chap. 3.

[12]Paris, D. T., and Hurd, F. K., *Basic Electromagnetic Theory*, McGraw–Hill, New York, 1969, Chap. 2.

[13]Blevins, R. D., *Formulas for Natural Frequency and Mode Shape*, Van Nostrand Reinhold, New York, 1979, Chap. 8.

[14]Goldstein, H., *Classical Mechanics*, Addison–Wesley, Cambridge, MA, 1951, Chap. 2.

[15]Meirovitch, L., *Elements of Vibration Analysis*, 2nd ed., McGraw–Hill, New York, 1986, Chaps. 7, 8.

G. M. Faeth
Editor-in-Chief